AD-A181 323 STUDIES IN THE COMPUTATION OF COMPRESSIBLE VISCOUS FLOWS(U) ARIZONA STATE UNIV TEMPE DEPT OF MECHANICAL AND AEROSPACE ENGINEERING K FUNG FEB 87 1/1

UNCLASSIFIED AFOSR-TR-87-0695 AFOSR-83-0071 F/G 1/1 NL

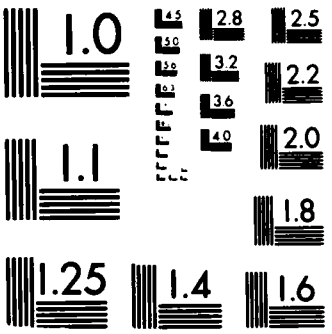
1.0
1.1
1.25
1.4
1.6
1.8
2.0
2.2
2.5
2.8
3.2
3.6
4.0
4.5
5.0
5.6
6.3
7.1
8.0
9.0
10.0

AFOSR-TR- 87-0695

Interim Scientific Report

AFOSR Grant No. 83-0071

February 15, 1986 to February 14, 1987

STUDIES IN THE COMPUTATION OF COMPRESSIBLE VISCOUS FLOWS

Submitted to:

Air Force Office of Scientific Research

Submitted by:

K.-Y. Fung, Associate Professor
Department of Aerospace & Mechanical Engineering

UNCLASSIFIED

SECURITY CLASSIFICATION OF THIS PAGE

REPORT DOCUMENTATION PAGE

1a. REPORT SECURITY CLASSIFICATION: UNCLASSIFIED	1b. RESTRICTIVE MARKINGS
2a. SECURITY CLASSIFICATION AUTHORITY	3. DISTRIBUTION/AVAILABILITY OF REPORT: APPROVED FOR PUBLIC RELEASE DISTRIBUTION IS UNLIMITED
2b. DECLASSIFICATION/DOWNGRADING SCHEDULE	
4. PERFORMING ORGANIZATION REPORT NUMBER(S)	5. MONITORING ORGANIZATION REPORT NUMBER(S): AFOSR-TR- 87-0695
6a. NAME OF PERFORMING ORGANIZATION: UNIV OF AZ; 6b. OFFICE SYMBOL (If applicable)	7a. NAME OF MONITORING ORGANIZATION: AFOSR/NA
6c. ADDRESS (City, State and ZIP Code): DEPT OF AERO AND MECH ENGR, UNIVERSITY OF AZ, TUCSON AZ 85721	7b. ADDRESS (City, State and ZIP Code): BUILDING 410, BOLLING AFB, DC 20332-6448
8a. NAME OF FUNDING/SPONSORING ORGANIZATION: AFOSR/NA; 8b. OFFICE SYMBOL (If applicable)	9. PROCUREMENT INSTRUMENT IDENTIFICATION NUMBER: AFOSR-83-0071
8c. ADDRESS (City, State and ZIP Code): BUILDING 410, BOLLING AFB, DC 20332-6448	10. SOURCE OF FUNDING NOS.

PROGRAM ELEMENT NO	PROJECT NO.	TASK NO.	WORK UNIT NO.
61102F	2307	A1	

11. TITLE (Include Security Classification): (U) STUDIES IN THE COMPUTATION OF COMPRESSIBLE VISCOUS FLOWS

12. PERSONAL AUTHOR(S): K-Y FUNG

13a. TYPE OF REPORT	13b. TIME COVERED	14. DATE OF REPORT (Yr., Mo., Day)	15. PAGE COUNT
ANNUAL	FROM _____ TO _____	FEB 1987	15

16. SUPPLEMENTARY NOTATION

17. COSATI CODES			18. SUBJECT TERMS (Continue on reverse if necessary and identify by block number)
FIELD	GROUP	SUB GR	
			TRANSONIC FLOW, COMPUTATIONAL AERODYNAMICS, VISCOUS-INVISCID INTERACTIONS

19. ABSTRACT (Continue on reverse if necessary and identify by block number)

The thin layer Navier-Stokes/Euler code has been modified to implement the method of viscous effect and truncation error. These effects can be injected into the solution of the Euler equations on a grid which is normally to course to account for the viscous effects in the boundary layer. Additionally, studies have been conducted to refine transonic flow computations. By a study of the possible local, near sonic solutions in the hodograph plane, singular solutions have been found which may bridge the gap between smooth shock free flow and the flow with embedded shocks.

20. DISTRIBUTION/AVAILABILITY OF ABSTRACT	21. ABSTRACT SECURITY CLASSIFICATION
UNCLASSIFIED/UNLIMITED ☒ SAME AS RPT ☐ DTIC USERS ☐	UNCLASSIFIED

22a. NAME OF RESPONSIBLE INDIVIDUAL	22b. TELEPHONE NUMBER (Include Area Code)	22c. OFFICE SYMBOL
HENRY E HELIN, CAPTAIN, USAF	202-767-4935	AFOSR/NA

DD FORM 1473, 83 APR — EDITION OF 1 JAN 73 IS OBSOLETE

UNCLASSIFIED

SECURITY CLASSIFICATION OF THIS PAGE

Interim Scientific Report

STUDIES IN THE COMPUTATION OF COMPRESSIBLE AND VISCOUS FLOWS

AFOSR Grant No. 83-0071

Submitted by:

K.-Y. Fung, Associate Professor
Department of Aerospace and Mechanical Engineering
College of Engineering and Mines
University of Arizona
Tucson, Arizona 85721

Submitted to:

Air Force Office of Scientific Research
Bolling Air Force Base
Washington, D.C. 20332
Attention: Dr. James D. Wilson

Contract Period
February 14, 1986 - February 15, 1987

SUMMARY

Report here are the research activities supported by AFOSR Grant N0. 83-0071 from February 15, 1986 to February 14, 1987.

On VISCOUS EFFECT INJECTION: a code has been assembled for either globle or local computation of flow over an airfoil. Using this code, we were able to show that viscous effects computed on a seperate, local grid can be injected into an inviscid solution of the Euler equations on a global grid. A paper on this work was presented at the AIAA 25th Aerospace Sciences Meeting in Reno last January. On REFINED TRANSONIC FLOW COMPUTATIONS: our computations of the flow over a circular cylinder with local refinement and an local analysis by Dr. Sobieczky, who visited and colaborated with us last summer, indicated the existence of shock free flow over a range of Mach number slightly greater than the critical value. Also our computations of the flow over an ellipse at an angle of attack showed that the circulation may not be arbitrary and is very sensitive to the amount of artificial viscosity and the grid. On THREE-DIMENSIONAL UNSTEADY TRANSONIC FLOW COMPUTATION WITH TEI: the modification of computer codes for this study has been completed. Preliminary results showed that a steady fine grid solution can be recovered on a coarse grid and the truncation error injected to render the fine grid solution is indeed very small except near the leading edge, the trailing edge, and the shock.

Three papers on our earlier works have been accepted for journal publication. Five masters/Ph.D. students have been supported fully or partially by this grant. The paper presented at the AIAA meeting is appended, and a brief description of the progress on each topic follows.

VISCOUS AND INVISCID INTERACTIONS

The thin-layer Navier-Stokes/Euler code, due to Steger and Pulliam, has been modified to implement the method of viscous effect and truncation error injection for computations of compressible flow over an airfoil. Viscosity can be turned on and off by a parameter in the code. Communications between solutions on different grids, i.e., the extraction of the boundary conditions for the local solution and the computation of truncation error for the refined global solution, are handled by an interpolation scheme designed for arbitrary curvillinear meshes.

This code and our viscous-inviscid interaction method were applied to compute viscous flow over a NACA0012 airfoil at subcritical Mach numbers. The results showed that viscous effects, as well as truncation error, can be injected into an inviscid solution of the Euler equations on a grid which normally is too coarse to account for the viscous effects in the boundary layer. However, we have not been able to move the boundaries of a local grid arbitrarily close to the body, due to an instability of the local solution. It is found in our studies that it is better, and more general, to prescribe pertubations of the Riemann invariants as boundary conditions than the Riemann invariants. More work needs to be done to overcome the difficult of imposing proper boundary conditions for the local solution.

A summary of this work was presented at the AIAA 25th Aerospace Sciences Meeting, January, 1987 in Reno, Nevada. A copy of the paper is in Appendix I.

REFINED TRANSONIC FLOW COMPUTATIONS

Our preliminary results of the flow over a cylinder at Mach numbers slightly greater than the critical value $M = 0.4$ showed that there seems to be a range of Mach number in which the flow is free of shocks, as Van Dyke conjectured by showing the convergence of a Rayleigh-Janzen type expansion carried to very high order. By a study of the possible local, near sonic solutions

in the hodograph plane, Sobieczky has found a singular solution which may bridge the gap between smooth shock-free flow and flow with embedded shocks. Though singular, this solution does not have the post-shock logarithmic singularity described by Oswatitsch and Zierep. Further refined computations of the local flow should reveal the existence of this singularity, which could have significant effects on the stability of the boundary layer.

We have carried out a series of computations of flow over ellipses at an incident with the free stream. Since the ellipse does not have a sharp trailing edge, the flow over it may assume any circulation, according to inviscid theory. However, the circulation of such a flow computed by a numerical scheme may depend sensitively on the truncation error due to discretization and the numerical viscosity added in order to stabilized the scheme. We have found converged numerical solutions with a negative lift for an ellipse at a positive angle of attack with the free stream. We have found that the circulation depends on the grid and the amount of numerical viscosity but surprisingly, not so much on the discretization method. It is hope that further studies and more refined computations will lead to a better understanding of the numerical solution of the Euler equations.

APPENDEX I

AIAA'87

AIAA-87-540

A Truncation Error Injection Approach to Viscous-Inviscid Interaction

B.D. Goble and K.-Y. Fung
The University of Arizona, Tucson, AZ

AIAA 25th Aerospace Sciences Meeting
January 12-15, 1987/Reno, Nevada

A TRUNCATION ERROR INJECTION APPROACH TO VISCOUS-INVISCID INTERACTION

B.D. Goble* and K.-Y. Fung**
Aerospace and Mechanical Engineering
University of Arizona, Tucson, Arizona 85721

Abstract

A numerical procedure which uses truncation error injection derived from a local fine grid solution or from a near body viscous solution is presented in the context of solving flow over an airfoil. A global solution on a coarse grid interacts with a solution calculated on a local fine grid which is fully enclosed within the global grid. The global solution passes boundary conditions and initial values to the local solution which, in turn, is used to form truncation error approximations. Truncation error is formed by operating with the global solution operator on the local grid solution which has been interpolated onto the coarse grid. The resulting space varying function is used as a forcing function in the explicit part of the global solver. This space varying function will be nonsero only in the region common to the local grid and the global grid. Both the local and the global solutions can be viscous or inviscid. The validity of this method is confirmed by comparison with results from a thin-layer Navier-Stokes code on a NACA 0012 airfoil at a low angle of attack.

I. Introduction

Computation of 2-D transonic flows over aerodynamic bodies has reached a stage where solutions to most reasonable problems can be found with some degree of accuracy. Naturally, there are many available approaches to finding these solutions. One of the more popular methods is to solve the Reynolds-averaged Navier-Stokes equations using finite difference methods. An advantage of this approach is that it can compute separated flows which have vorticity convecting into the inviscid region. Also, the code tends to be very robust, able to calculate a wide variety of cases without having to change more than a few parameters. However, due to the wide range of length scales present in the problem and the difficulty of producing an adequate grid to resolve them, these codes are very expensive when it comes to computer resources and require a fast computer with extensive memory in order to be practical.

Another approach to solving these types of transonic flow problems is often called viscous-inviscid interaction. A compressible boundary layer code is coupled with some type of inviscid flow solver through a complex interaction scheme. The boundary layer code calculates the viscous flow near the body and passes boundary conditions to the inviscid flow solver, usually a full potential code, which in turn calculates the outer flow and passes boundary conditions back to the boundary layer scheme. The boundary conditions which are typically passed are displacement thickness or transpiration velocity from the boundary layer code to the potential code and wall pressure distribution from the potential code back to the boundary layer code. This approach is much more efficient than the Navier-Stokes solvers, both in CPU time and in memory requirements. Also, since two grids are used, it is easier to tailor the grids to capture the relevant length scales in each region. However, this approach is not as robust as the Navier-Stokes approach. The algorithm breaks down in cases with large separation regions since the boundary layer code cannot calculate this flow situation. Also, the potential flow code cannot convect vorticity away from the body or wake region and tends to overpredict shock strengths. To counteract these last two problems, Steger and Van Dalsem[1] incorporated a vector potential code due to Chaderjian[2] in place of the usual full potential code, thus including vorticity transport in the free field and giving more accurate shock fitting. New boundary conditions were also used for the inviscid part of the interaction. The boundary layer equations generate vorticity, entropy, and changes of stagnation enthalpy effects which are used as inputs to the inviscid flow solver.

This paper discusses an approach to viscous-inviscid interaction which is similar to that used by Steger and Van Dalsem. This approach is based on truncation error injection, which will be explained first. Then its application to viscous-inviscid interaction will be discussed followed by a brief discussion of the 2-D interpolation scheme used to restrict the fine grid solutions to the global coarse grid. Section IV contains some details on the current implementation of the approach and Section V discusses the boundary conditions being used. Section VI presents the inviscid results from a NACA0012 airfoil test case and then the viscous results.

II. Theory

Truncation error occurs when a differential equation is discretised on a grid with finite mesh spacing. To illustrate what is meant by truncation error injection, a simple symbolic approach will be used. Suppose that the differen-

* Research Assistant, Student member AIAA
** Associate Professor, Member AIAA

tial equation to be solved can be written in operator form as

$$L\Phi = 0 \tag{2.1}$$

where L is a continuous differential operator and Φ is the exact continuous solution. Now finite difference L on some grid with characteristic mesh spacing h to get

$$L_h\Phi - T.E._h = 0 \tag{2.2}$$

where L_h is a discrete operator and $T.E._h$ is the truncation error associated with the differencing. Typically, in solving this equation numerically, $T.E._h$ is assumed to be small and is neglected. However, it can be significant. If $T.E._h$ was known a priori, the exact solution could be found. When truncation error injection is used, $T.E._h$ is estimated using information from a finer grid.

First, difference L on a grid with characteristic mesh spacing k, where $k < h$, to get

$$L_k\Phi - T.E._k = 0. \tag{2.3}$$

Now neglect $T.E._k$, which is smaller than $T.E._h$, and solve to get a solution Φ_k that approximates Φ to $O(k^n)$ where n is the order of the scheme. Now restrict Φ_k onto the coarse grid to get Φ_k^h. Operate on the resulting solution vector with the coarse grid operator to define a new quantity $T.E._k^h$ as

$$T.E._k^h = L_h\Phi_k^h \tag{2.4}$$

where $T.E._k^h$ is a spatially varying function which is an estimate of the local truncation error. Now inject the estimated truncation error onto the right hand side of the original equation as a forcing function and solve

$$L_h\Phi_h = T.E._k^h. \tag{2.5}$$

Obviously, if the fine grid and coarse grid are the same, Φ_h will converge to Φ_k^h and nothing is gained. However, suppose the fine grid is strictly a local grid, say around a shock or encompassing a boundary layer or some other region of large gradients. The function $T.E._k^h$ will then be nonsero only at the coarse grid nodes lying within the boundaries of the local fine grid. In this case, Φ_h will converge to a solution influenced by Φ_k^h but not identical to it. The difference between Φ_h and Φ_k^h in the patch is dependent upon such factors as the size of the patch and boundary conditions used. However, the overall solution will be improved by the injected truncation error in the patch since Φ_k^h is a better solution than Φ_h in the patch.

Now, look at how this approach can apply to an interaction scheme. Suppose that the fine grid solution is a viscous solution, provided by either a boundary layer solver or a Navier-Stokes solver, and the global solver is an inviscid solver such as an Euler solver or a vector-potential solver. The truncation error term formed in Eqn.(2.4) will then contain viscous information as well as truncation error information. The injection of this term as a forcing function will cause the flow to feel the viscous effects as calculated on the fine grid. The usage of two uncoupled grids also enables the relevant length scales to be captured more efficiently than if only one grid were used.

The term $T.E._k^h$ also contains information about the truncation error incurred in differencing the inviscid terms. This information will improve the accuracy of the convective terms on the coarse grid. Accuracy is lost in the boundary layer when the grid is coarsened in the normal direction. The truncation error information helps to reduce the loss of accuracy due to the increased mesh spacing.

III. Interpolation Scheme

In the implementation of this scheme, the fine grid solution must be interpolated from the local grid in one curvilinear coordinate system to the global grid in another curvilinear coordinate system and back again. This interpolation is handled by a routine that will interpolate a function of two variables from one general grid to another general grid. Some function $Q1$ is known as $Q1(X1, Y1)$ and as $Q1(\xi, \eta)$, where $(X1, Y1)$ are the physical coordinates of grid 1 and (ξ, η) are the coordinates in the corresponding computational plane. First of all, each point in grid 2 is located in grid 1 with a nearest neighbor search routine. The mappings $Q1(\xi, \eta)$, $X1(\xi, \eta)$, and $Y1(\xi, \eta)$ are approximately found using a local bicubic surface to represent the evenly spaced data. The point in grid 1 closest to the current point in grid 2 is used as the origin of the bicubic surface and as an initial guess to a Newton type sero finding routine. Say $(\hat{\xi}, \hat{\eta})$ are the coordinates of the nearest neighbor point. Then $X1(\hat{\xi}, \hat{\eta})$ and $Y1(\hat{\xi}, \hat{\eta})$ are found as well as the partial derivatives with respect to ξ and η at that point. This new data is used in the Newton routine to drive to sero the functions

$$f(\hat{\xi}, \hat{\eta}) = XPT - X1(\hat{\xi}, \hat{\eta})$$
$$g(\hat{\xi}, \hat{\eta}) = YPT - Y1(\hat{\xi}, \hat{\eta})$$

where (XPT, YPT) are the coordinates of the current point in grid 2. At convergence, we know the coordinates (ξ^*, η^*) of the current grid 2 point in the computational domain. Using the mapping found earlier, the value $Q2(\xi^*, \eta^*)$ can now be found.

IV. Implementation

The thin-layer Navier-Stokes/Euler code ARC2D, due to Steger and Pulliam, is being used to implement the method due to its familiarity, ease of use and the fact that it performs both inviscid and viscous simulations. Details of this code will not be presented here as it is discussed at length elsewhere.[3-6] The code was modified to iteratively

solve the coupled systems. First, a converged solution is found on the global grid. This solution is then interpolated onto the local grid and a solution is found to some degree of convergence. This solution is then restricted back to the global grid. The interpolated solution is then operated on by the various operators that form the explicit side of the calculation, i.e. the boundary conditions, the convective terms and the artificial dissipation terms. The viscous operators can also be used if it is desired to use the thin-layer Navier-Stokes equations instead of the Euler equations as the global solver. The resulting residual is saved as an estimate of the truncation error due to the difference in the two grids and/or the solvers. The global solution is then found as usual except that at each step, the stored forcing function is subtracted from the explicit side of the operator so that at convergence the combined residual is zero. The implicit side is not changed in any way. This solution is then interpolated back to the local grid and the process is repeated until some appropriate measure of convergence is satisfied.

V. Boundary Conditions

The boundary conditions being used in the code are very similar to those used in the original code.[6] The wall and wake conditons are the same. The far field characteristiclike boundary conditions are slightly modified so that they may also be used for the local grid. As used in Ref. 6, the locally one dimensional Riemann invariants are

$$R_1 = V_n - \frac{2a}{\gamma - 1}$$

$$R_2 = V_n + \frac{2a}{\gamma - 1}$$

where V_n is the velocity normal to the far field boundary. For an inflow boundary, $V_n < 0$ and R_1, the tangential velocity, V_t, and an approximation to the entropy, $S = \frac{P}{\rho^\gamma}$ are all specified from free stream conditions. R_2 is extrapolated from the interior. For outflow, $V_n > 0$ and R_2, V_t and S are extrapolated from the interior. R_1 is then specified from freestream conditions. From these quantities, the four conservative variables ρ, ρu, ρv, and e can be found.

This approach has been modified slightly. Define perturbation Riemann invariants as

$$\Delta R_1 = \Delta V_n - \frac{2\Delta a}{\gamma - 1}$$

$$\Delta R_2 = \Delta V_n + \frac{2\Delta a}{\gamma - 1}$$

where, for example,

$$\Delta V_n = V_n^N - V_n^{N-1}$$

and V_n^N is evaluated at the N^{th} time step at freestream conditions for ΔR_1 and at the first grid line inside the boundary for ΔR_2. It is easy to see that for constant free stream conditions, $\Delta R_1 = 0$ and all that is needed is ΔR_2. For inflow, we have

$$V_t^N = V_t^{N-1}$$

$$S^N = S^{N-1}$$

evaluated at the boundary and for outflow we have

$$V_t^N = V_t^{N-1} + \Delta V_t$$

$$S^N = S^{N-1} + \Delta S$$

evaluated as previously described. These boundary conditions give virtually identical results as the original versions when used for far field conditions in a single grid calculation and give better results when used for the outer boundaries of the local grid.

VI. Results

The method was applied to a NACA0012 airfoil at $M_\infty = 0.6$, $\alpha = 1.0$ deg on a coarse grid (193x33 points) and a fine grid (225x49 points) which cover the same physical domain. Viscous and inviscid cases were run on each grid for comparison with the results from the present investigation. The cases on the fine grid were interpolated to the coarse grid using the interpolation routine. These solutions were then used to form the forcing terms for the coarse grid calculations. Three calculations were made, an inviscid run forced by the fine grid inviscid solution (FIICGR3), an inviscid run forced by the fine grid viscous solution (FVICGR3), and a viscous run forced by the fine grid viscous solution (FVVCGR3). An inviscid run was also made on the fine grid using the fine grid viscous solution to form the forcing function (FVICGR1).

Coefficients of Lift, Drag, and Moment			
	C_L	C_D	C_M
ICGR1	0.15827	0.00015	-0.00081
FIICGR3	0.15816	0.00010	-0.00071
VCGR1	0.14555	0.00197	0.00095
FVICGR3	0.14558	0.00194	0.00093
FVVCGR3	0.14558	0.00194	0.00093
FVICGR1	0.14555	0.00197	0.00095

TABLE 1

$M_\infty = 0.6$, $\alpha = 1.0$ deg, Inviscid.
Global and Local grids have same domain.

These four runs were made using the fine grid solutions as initial conditions to check the interpolation routine and the implementation of the method. Each calculation converged in one step as it should. These resulting solutions were then compared with the fine grid viscous solution

(VCGR1) and the fine grid inviscid solution (ICGR1) in terms of C_L, C_D, and C_M. Table 1 shows the C_L, C_D and C_M values due to integrating C_P around the body for all the cases. The agreement between the appropriate cases is good. Therefore, we can conclude that the interpolation routine is working well and we can proceed.

The next step was to implement local to global interaction to solve inviscid flow about a NACA0012 airfoil at $M_\infty = 0.5$, $\alpha = 2.0$ deg. A 161x33 grid with a minimum $\Delta Y = 0.002$ was used for the global grid. Several different local grids were used. They were all derived from either a 225x49 grid with a minimum $\Delta Y = 0.0005$ or a 249x65 grid with a minimum $\Delta Y = 0.0001$. The local grids were formed by taking the first n lines from the body in the full grid. Each of the cases was restarted using the inviscid solution on the global grid as an initial condition. The following tables show values for C_L, C_D and C_M as found on the local grid.

Coefficients of Lift, Drag, and Moment			
	C_L	C_D	C_M
225x49	0.27847	0.00034	-0.00176
225x37	0.27824	0.00035	-0.00176
225x35	0.27835	0.00034	-0.00176
225x33	0.27847	0.00035	-0.00177
225x31	0.27845	0.00034	-0.00177
225x29	0.27851	0.00038	-0.00179
225x27	0.27845	0.00040	-0.00180

TABLE 2

$M_\infty = 0.5$, $\alpha = 2.0$ deg, Inviscid. Local grid based on 225x49 grid. Min $\Delta Y = 0.0005$

Table 2 shows the lift and drag coefficients for the cases using local grids based on the 225x49 grid. The first entry in the table is the single grid solution obtained on the full 225x49 grid. The next two cases agree well with these results. Beginning with the third case, the values start to diverge from the single grid results. The values for C_L do not appear to follow any logical progression as the size of the fine grid is reduced, but all values shown are within 0.1% of the 225x49 case. Actually, the closest solution is the 225x33 case. No explanation for this behavior has been found. A 225x25 case was also attempted. The solution appeared to converge very well and then suddenly diverged very rapidly. It was determined that this behavior was due to the fine grid outer boundary being too close to the airfoil.

Fig. 1 shows the Mach number contours for the 225x31 case as displayed on the global grid. The gridline shown is the approximate outer limit of the local grid. The contours are continuous across the grid boundary indicating that the local solution is blending smoothly with the global solution. Comparing Fig. 1 with Fig. 2, which shows the Mach number contours as calculated on the 249x65 grid, we can see that the agreement with the fine grid solution is quite good.

Coefficients of Lift, Drag, and Moment			
	C_L	C_D	C_M
249x65	0.27892	0.00030	-0.00175
249x47	0.27857	0.00030	-0.00175
249x45	0.27876	0.00031	-0.00177
249x43	0.27847	0.00035	-0.00177
249x41	0.27845	0.00034	-0.00177
249x39	0.27851	0.00038	-0.00179

TABLE 3

$M_\infty = 0.5$, $\alpha = 2.0$ deg, Inviscid. Local grid based on 249x65 grid. Min $\Delta Y = 0.0001$

Table 3 shows the lift and drag coefficients for the cases using local grids based on the 249x65 grid. The first entry is the single grid result for the 249x65 grid. The results shown exhibit the same pattern as the previous case. The best agreement in C_L occured on the 249x45 grid. All C_L values are within 0.2% of the fine grid value. The accuracy for the C_D and C_M values does increase as the size of the fine grid is increased. In this case, the smallest grid that could be used without the solution diverging was a 249x39 grid. Fig. 3 shows the C_P contours for the 225x45 case. Again, the solution appears to be continuous across the local grid boundary. The C_P contours for the 249x65 case are shown in Fig. 4. Agreement between the two cases is good. Fig. 5 shows the entropy contours for the 249x45 case. All entropy generation is taking place at the leading edge or elsewhere along the body. The local grid boundary is not generating any entropy. Fig. 6 shows the entropy contours for the 249x65 case.

Coefficients of Lift, Drag, and Moment			
	C_L	C_D	C_M
225x49	0.25084	0.01098	0.00232
225x39	0.25141	0.01095	0.00234
225x37	0.25133	0.01094	0.00234
225x35	0.25135	0.01092	0.00234
225x33	0.25081	0.01094	0.00232
225x31	0.25118	0.01098	0.00228
193x49	0.24974	0.01261	0.00256

TABLE 4

$M_\infty = 0.5$, $\alpha = 2.0$ deg, $Re = 10^6$. Local grid based on 225x49 grid. Min $\Delta Y = 0.0005$

The code was next applied to subcritical viscous flow about a NACA0012 airfoil at $M_\infty = 0.5$, $\alpha = 2.0$ deg,

and $Re = 10^6$. A 193x49 global grid with a minimum $\Delta Y = 0.00006$ was used in conjunction with local grids derived from a 225x49 grid with a minimum $\Delta Y = 0.00002$. The global solution was found using the Euler solver and viscous type boundary conditions while the local solution was found assuming turbulent viscous flow. An algebraic mixing length model due to Baldwin and Lomax[7] was used to approximate the turbulent effects. Transition was assumed to occur at 10% of chord on both the top and bottom of the airfoil.

The values for C_L, C_D and C_M for the viscous cases are shown in Table 4. Again the values of C_L do not follow any recognisable pattern as the local grid size is changed. The best agreement occurs in the 225x33 case; all others are within 0.3% of the single grid solution. Unlike the inviscid results, here the C_D and C_M values also do not follow any sort of pattern. The 225x33 case gives the best overall agreement for the three coefficients. The values for the 193x49 case shown are for the solution as found on the global grid alone without a local grid and were included for comparison. Fig. 7 shows the Mach contours from the 225x33 case. Note the smoothness of the contours across the local grid boundary and the good agreement with the single grid results shown in Fig. 8. The plots of C_P shown in Fig. 9 and Fig. 10 also agree very well.

VII. Conclusions

These results show the validity of this approach to solving inviscid or viscous flow over airfoils. More work needs to be done to understand better where to place the outer boundary of the local grid. The location of the outer boundary of the local grid, beyond some threshold, does not appear to have any predictable effect on the accuracy of C_L. Except in the viscous case, increasing the size of the local grid did improve the results for C_D and C_M. Also, with more understanding on how the two grids interact, better grids can be generated to put more resolution where it is needed.

Acknowledgements

This research was carried out at NASA Ames Research Center, Moffett Field, California and at the Computational Fluid Mechanics Laboratory of the Aerospace and Mechanical Engineering Department at the University of Arizona. The authors would like to thank NASA for its help and support in conducting the work presented here. We are grateful to NASA for support under Interchange Number NCA2-107, and to the Air Force under Contract Number AFOSR-83-0071. We are also grateful to Dr. Terry Holst for his permission to use the NASA Ames CRAY-XMP computer for this and other studies related to the traineeship program. We are especially grateful to Dr. Tom Pulliam for his guidance and instruction during the first author's time at Ames.

References

1. Steger, J. L. and Van Dalsem, W. R., "Developments in the Simulation of Separated Flows Using Finite Difference Methods," Proceedings of the Third Symposium on Numerical and Physical Aspects of Aerodynamic Flows," California State University, Long Beach, California, Jan. 21-24, 1985.

2. Chaderjian, N. M. and Steger, J. L., "The Numerical Simulation of Steady Transonic Rotational Flow Using a Dual Potential Formulation," AIAA Paper 85-0368, 1985.

3. Steger, J. L., "Implicit Finite Difference Simulation of Flow about Arbitrary Two Dimensional Geometries," AIAA J., Vol. 16, No. 7, July 1978, pp. 679-686.

4. Pulliam, T. H. and Steger, J. L., "On Implicit Finite Difference Simulations of Three Dimensional Flows," AIAA J., Vol. 18, No. 2, Feb. 1980, pp. 159-167.

5. Pulliam, T. H. and Steger, J. L., "Recent Improvements in Efficiency, Accuracy, and Convergence of Implicit Approximate Factorisation Algorithms," AIAA Paper 85-0360, presented at the 23rd Aerospace Sciences Meeting, Reno, Nev., Jan. 1985.

6. Pulliam, T. H., "Euler and Thin Layer Navier-Stokes Codes : ARC2D, ARC3D, Notes for Computational Fluid Dynamics User's Workshop," UTSI E02-4005-023-84, March 1984.

7. Baldwin, B. S., and Lomax, H., "Thin Layer Approximation and Algebraic Model for Separated Turbulent Flows," AIAA Paper No. 78-257(1978).

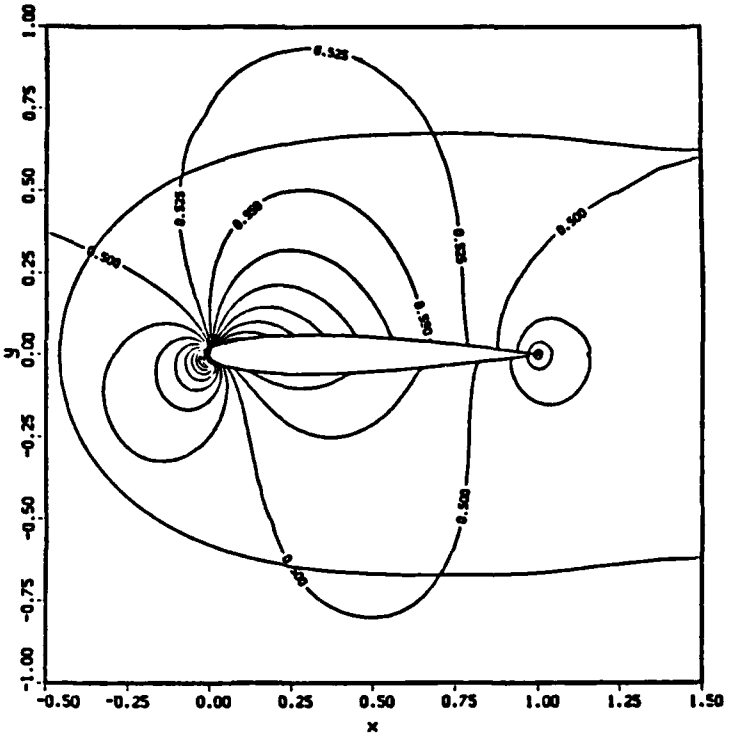

Fig. 1 Mach Number Contours. M_∞ = 0.5, α = 2 deg, 225x31 local grid, 161x33 global grid.

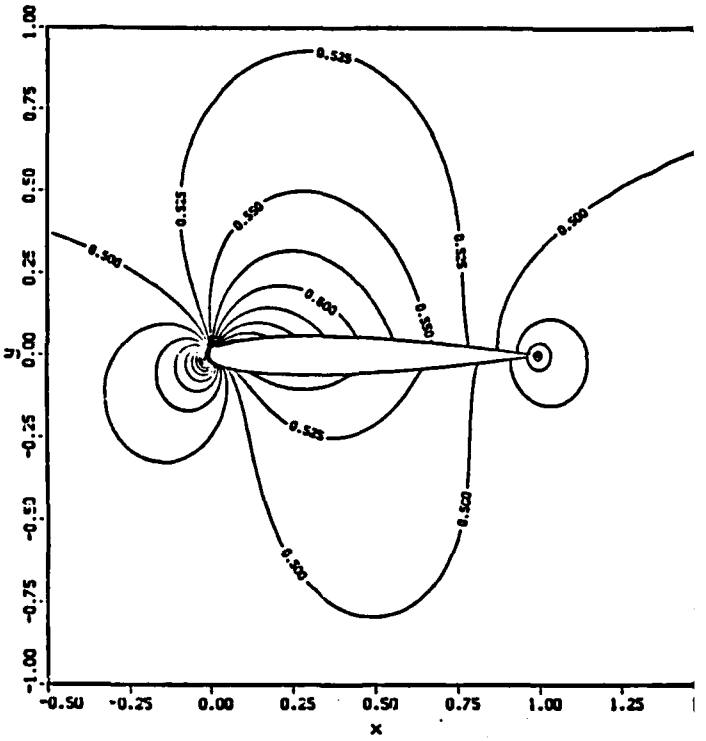

Fig. 2 Mach Number Contours. M_∞ = 0.5, α = 2 deg, 249x65 single grid.

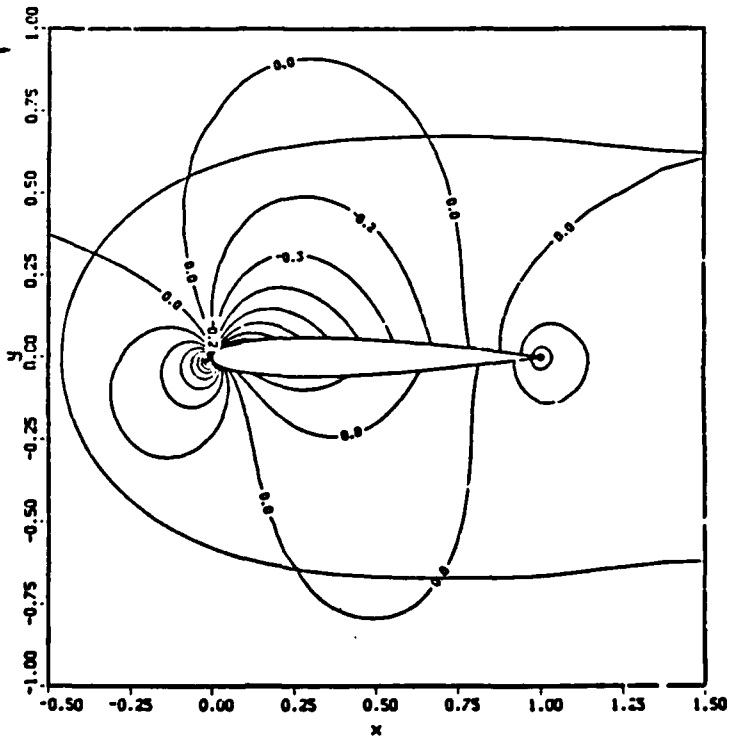

Fig. 3 C_p Contours. M_∞ = 0.5, α = 2 deg, 249x45 local grid, 161x33 global grid.

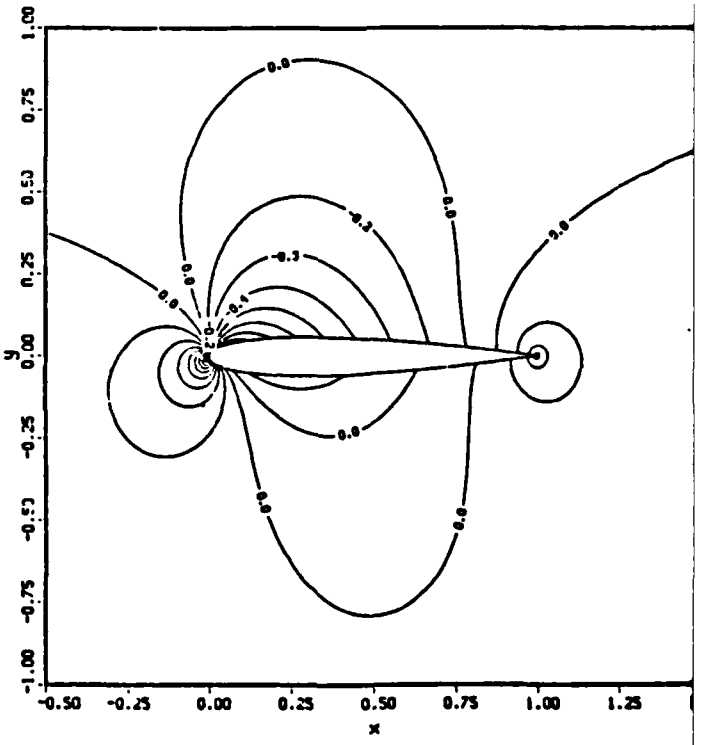

Fig. 4 C_p Contours. M_∞ = 0.5, α = 2 deg 249x65 single grid.

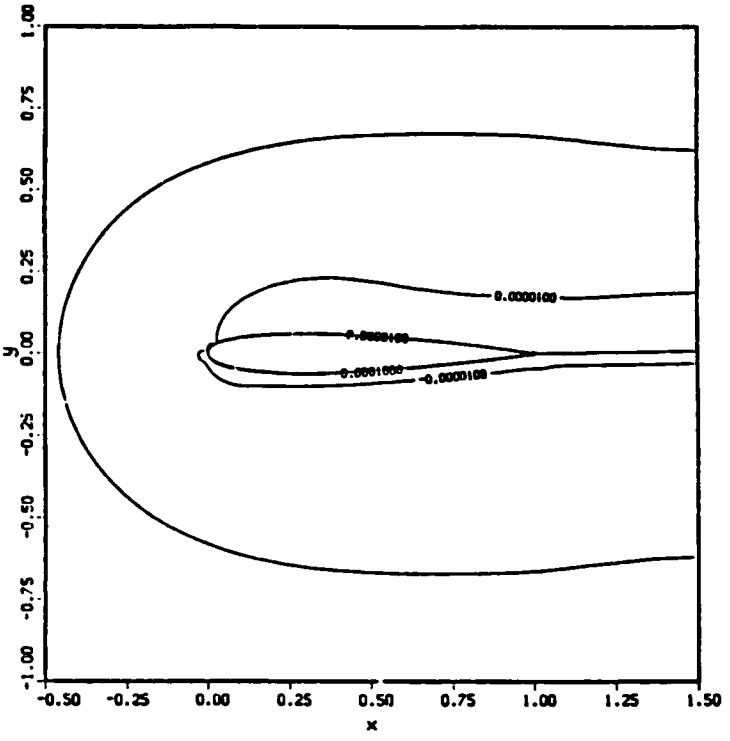

Fig. 5 Entropy Contours. $M_\infty = 0.5$, $\alpha = 2$ deg, 249x45 local grid, 161x33 global grid.

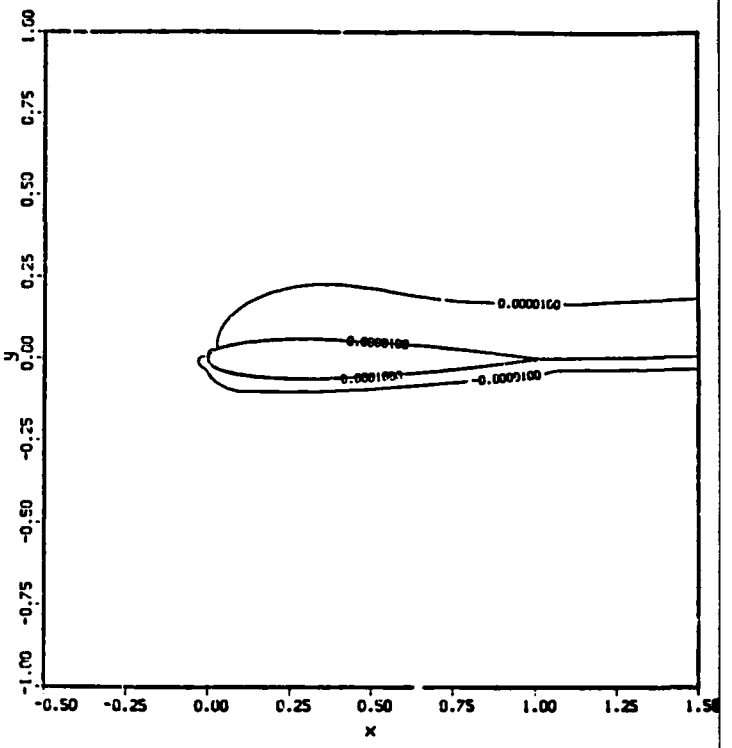

Fig. 6 Entropy Contours. $M_\infty = 0.5$, $\alpha = 2$ deg, 249x65 single grid.

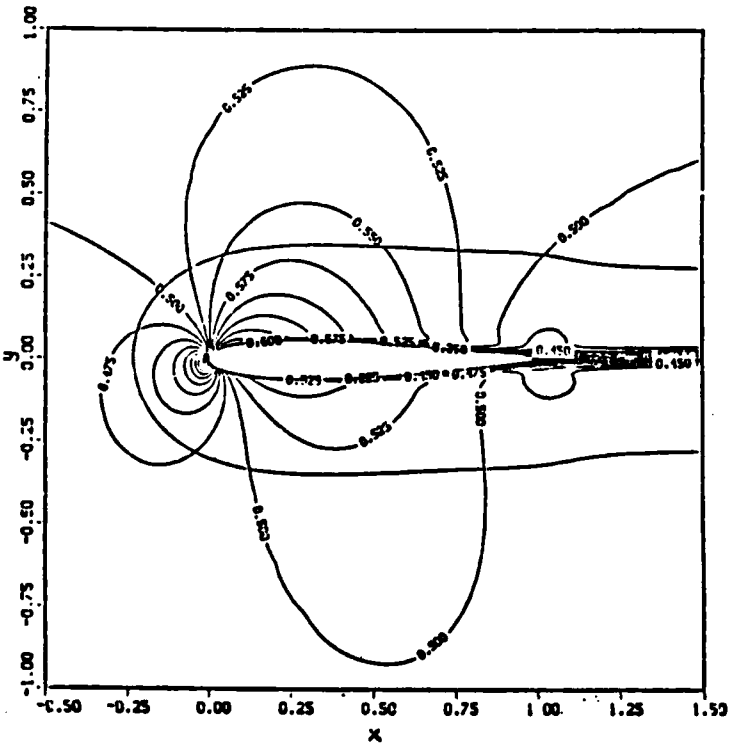

Fig. 7 Mach Number Contours. $M_\infty = 0.5$, $\alpha = 2$ deg, 225x33 local grid, 193x49 global grid.

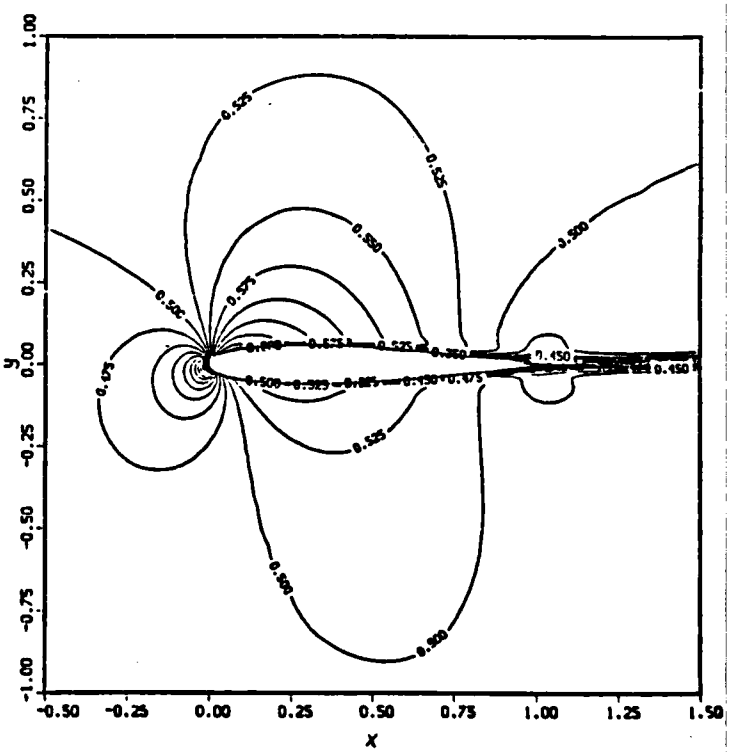

Fig. 8 Mach Number Contours. $M_\infty = 0.5$, $\alpha = 2$ deg, 225x49 single grid.

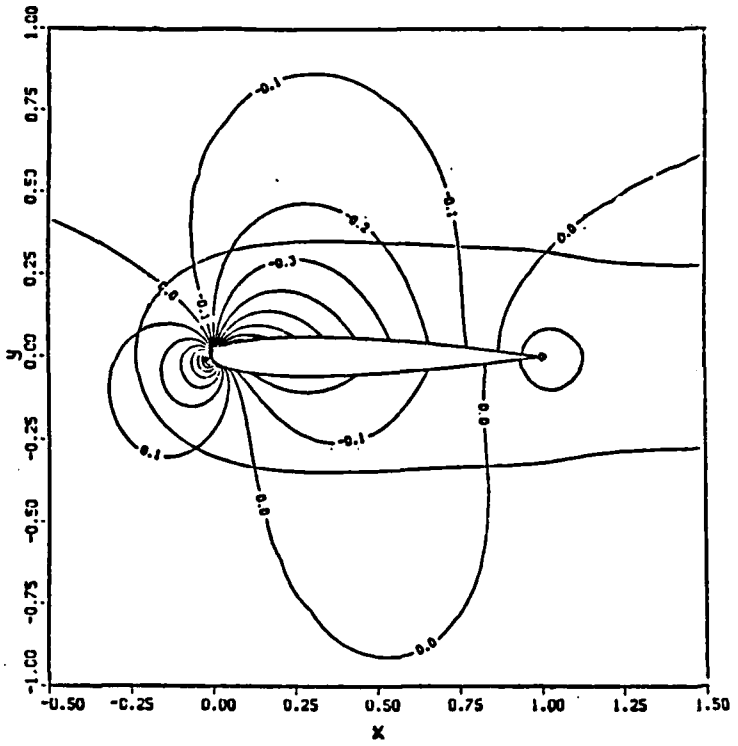

Fig. 9 Cp Contours. M_∞ = 0.5, α = 2 deg, Re = 10^6, 225x33 local grid, 193x49 global grid.

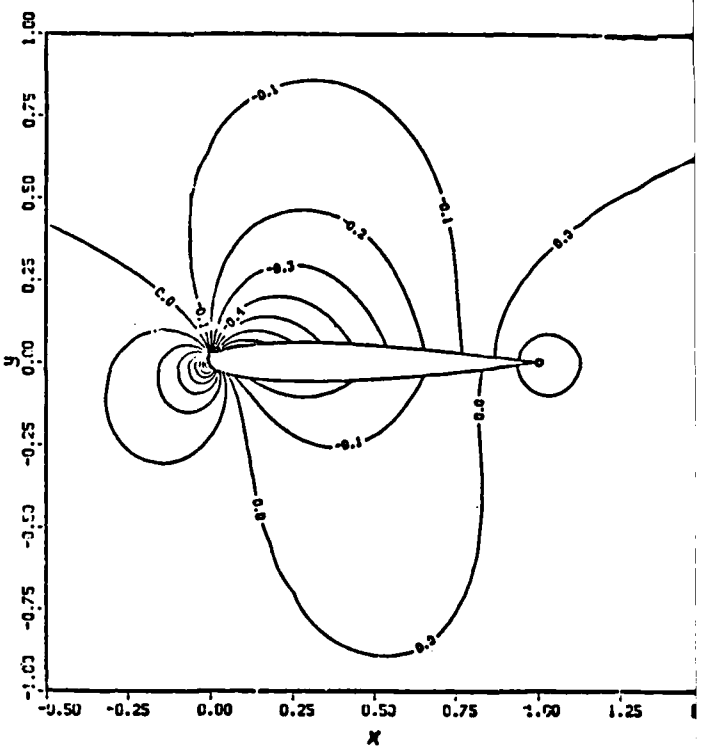

Fig. 10 Cp Contours. M_∞ = 0.5, α = 2 deg Re = 10^6, 225x49 single grid.

END

7-87

DTIC